





Cite this: *Analyst*, 2019, **144**, 954

# Molecular profiling of single axons and dendrites in living neurons using electrosyringe-assisted electrospray mass spectrometry†

Mingchen Xu,<sup>a</sup> Rongrong Pan,<sup>a</sup> Yue Zhu,<sup>b</sup> Dechen Jiang <sup>\*a</sup> and Hong-Yuan Chen <sup>\*a</sup>

The molecular profiling of single axons and dendrites in living neurons could provide important information for the better understanding of neuron function. Here, electrosyringe-assisted electrospray mass spectrometry (MS) is established for the first time to achieve intracellular sampling from one axon or dendrite in living neurons for mass spectrometric analysis. The key is the insertion of a ~130 nm capillary tip into one axon or dendrite to load the cytosol through electro-osmotic flow. The ionization efficiency from the nano-capillary is enhanced to guarantee mass spectrometric analysis of multiple components from the axon and dendrite. Higher levels of pyroglutamic acid and glutamic acid are revealed in the axon compared to in the body and dendrite. This uneven distribution is in accordance with the accumulation of neurotransmitters in the axon for information delivery. The achievement of electrosyringe-assisted electrospray MS is to unveil the molecular distribution in the whole living neuron, which offers the feasibility to deeply investigate molecular communication between the axon/dendrite and the body inside neurons.

Received 15th March 2018,

Accepted 30th July 2018

DOI: 10.1039/c8an00483h

[rsc.li/analyst](http://rsc.li/analyst)

## Introduction

A typical neuron consists of one body, a long axon and several short and highly branched dendrites. Axons and dendrites function differently; the dendrites receive information from other neurons and the axon delivers information.<sup>1,2</sup> The molecular profiling of a single living neuron, including the body, the axon and dendrites, could provide more elegant information about molecular distribution and function inside the cells that facilitates the better elucidation of information delivery among neurons.<sup>3,4</sup> Since the diameters of the axon and dendrites in mammalian neurons are ~1 μm, a technique with high spatial resolution is needed. Currently, super-resolution fluorescence microscopy has circumvented the limits of light diffraction and mapped molecules with subcellular spatial resolution below 200 nm.<sup>5–8</sup> However, fluorescence imaging relying on binding between probes and target molecules has

difficulties profiling multiple intracellular molecules, or revealing unknown molecules inside cells.<sup>9,10</sup>

Mass spectrometry (MS) is an analytical technique that ionizes chemical species and sorts the ions based on mass to charge ratio, which provides information about molecular weight and structure. No molecular information is needed in advance, making MS a suitable strategy for the deep-study of cellular metabolites.<sup>11–16</sup> Secondary ion mass spectrometry (SIMS) ionization<sup>17,18</sup> and matrix-assisted laser desorption/ionization (MALDI)<sup>19–21</sup> have been performed for the simultaneous sampling and ionization of single cells. A highest spatial resolution of less than 50 nm was reported using SIMS. However, due to the direct application of the ion beam or laser/matrix to the cells, it is challenging to utilize these approaches for the analysis of single living cells.<sup>17,18</sup> For living cells, electrospray ionization (ESI) based techniques have been developed to complete sampling from living cells, and then to conduct the ionization. Different strategies, including laser ablation,<sup>22–24</sup> single-probes,<sup>25–27</sup> live single-cell video-MS,<sup>28–30</sup> capillary electrophoresis<sup>31–34</sup> and patch clamping,<sup>35,36</sup> have been utilized for sampling. The currently spatial resolution of sampling for these above-mentioned ESI based techniques is on the micrometer level. Therefore, this restricts the application of ESI to the study of subtle cellular parts, such as single axons or dendrites. The latest coupling of scanning near-field optical microscopy (SNOM) or atomic force microscopy (AFM) with MS pushes spatial resolution down to

<sup>a</sup>The State Key Lab of Analytical Chemistry for Life Science, School of Chemistry and Chemical Engineering, Nanjing University, Nanjing, Jiangsu 210093, China.

E-mail: [dechenjiang@nju.edu.cn](mailto:dechenjiang@nju.edu.cn), [hychen@nju.edu.cn](mailto:hychen@nju.edu.cn); Tel: +86-25-89684846

<sup>b</sup>Jiangsu Key Laboratory for High Technology Research of TCM Formulae and Jiangsu Collaborative Innovation Center of Chinese Medicinal Resources Industrialization, Nanjing University of Chinese Medicine, Nanjing, Jiangsu 210093, China

†Electronic supplementary information (ESI) available: Characterization of ionization efficiency and more spectra and tables for the tentative substance assignment in mass spectra. See DOI: 10.1039/c8an00483h

nanometers,<sup>37,38</sup> while further development is needed to collect intracellular information.

Recently, Baker's group reported a nano-capillary with the tip opening less than 100 nm as an electrospray ionization emitter for ESI-MS.<sup>39</sup> The nano-tip was proven to assist greater droplet charging, which was highly beneficial for ion formation during mass spectrometric analysis. Moreover, the electrospray from the nano-tip was observed to be more tolerant of the salted buffer. All these features offer the feasibility of coupling a nano-capillary with ESI-MS for nanometer-scale analysis. Considering the difficulty of mechanically pumping liquid outside the nano-tip, Mirkin's group developed an electrosyringe to egress/ingress attolitres of liquid into/from the nano-capillary through electro-osmotic flow (EOF).<sup>40</sup> The volume was controlled by the applied voltage and time, and was not restricted by the size of the capillary orifice. In that approach, the organic solvent was loaded into the capillary and a two-phase (liquid–liquid) interface was formed at the capillary tip. Our group continued to electrochemically load single lysosomes from one mammalian cell into the nano-capillary for the analysis of glucosidase activity.<sup>41</sup> Similarly, small molecules (*e.g.* cholesterol), mRNA and mitochondria were isolated from single living cells using this electrosyringe.<sup>42–44</sup> Since the extra- and inner-capillary solutions are aqueous, no liquid–liquid interface is formed at the tip, which is different to Mirkin's model.

In this work, the electrosyringe is adapted in an electrospray ionization emitter to achieve ESI mass spectrometric analysis of one axon and dendrite from single living neurons. The nano-capillary with a tip opening of ~130 nm was positioned inside one axon or dendrite. Then, a small negative voltage was applied to a metal wire in the nano-capillary to initiate EOF for the ingress of cytosol (Fig. 1A). Afterwards, the nano-capillary tip was relocated near the inlet of the mass spectrometer and a high voltage was introduced to the metal wire to start the electrospray (Fig. 1B). During the whole process, the species were retained in the liquid and high ionization efficiency was guaranteed to realize the analysis of trace amounts of molecules in cytosol. The achievement of electrosyringe assisted ESI MS will provide a specific strategy for the molecular profiling of axons/dendrites/bodies in living neurons.

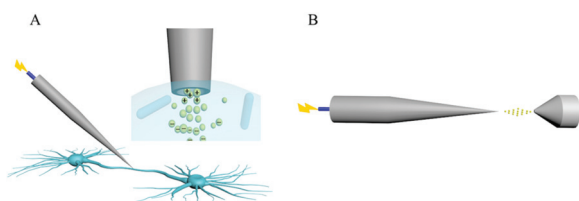


**Fig. 1** Schematic diagrams of (A) the electrosyringe for loading sample into the nano-capillary; and (B) the electrospray of the loaded sample for MS analysis.

## Experimental

### Chemicals and cell cultures

Borosilicate glass (BF100-58-10) was purchased from Sutter Instrument (USA). All chemicals were from Sigma-Aldrich, unless indicated otherwise. Primary cultured rat hippocampal neurons were isolated from a cortical neuron primary culture of mouse embryos at day 13.5, following our previous work.<sup>45</sup> The cells were cultured in medium (neurobasal medium, supplemented with 0.5 mM GlutaMAX and 1x B27). HeLa cells were obtained from the Institute of Biochemistry and Cell Biology, Shanghai Institute for Biological Science of the Chinese Academy of Sciences (Shanghai, China). HeLa cells were seeded in DEME/high glucose medium supplemented with 10% fetal bovine serum (FBS) and 1% antibiotics (penicillin/streptomycin). All cultures were maintained at 37 °C under a humidified atmosphere containing 5% CO<sub>2</sub>. The epidermis of *Allium cepa* was obtained using tweezers and positioned in a Petri dish with 1× phosphate buffered saline (PBS, including 137 mM NaCl, 2.7 mM KCl, 10 mM Na<sub>2</sub>HPO<sub>4</sub> and 2 mM KH<sub>2</sub>PO<sub>4</sub> at pH 7.4).

### Instrumentation

The electrosyringe assisted ESI MS was assembled with a nano-capillary, a metal wire, a voltage generator and a mass spectrometer. The nano-capillary with a tip opening of ~130 nm was reproducibly pulled using P-2000 apparatus (Sutter Instrument). A Pt wire used as the metal wire in the nano-capillary was connected to an electrochemical station (CHI 660, CH Instruments, USA) to introduce the voltage for sampling. An Ag/AgCl electrode was used as the reference electrode. After sampling, the nano-capillary was relocated near the inlet of a Q-TOF mass spectrometer (Agilent 6530B Q-TOF, Agilent Technologies, Inc. USA). A voltage of 2500 V was applied to the Pt wire using a high voltage generator (Dongwen High-Voltage Power Inc. China) for electrospraying.

### Single cell analysis

The nano-capillary was mounted on a 3D translation stage to achieve insertion into one *Allium cepa* cell, living HeLa cell or neuron part (body, axon or dendrite) for sampling. Prior to insertion, the cells were washed and re-cultured in a Petri-dish containing 1× PBS. During the insertion, a small negative voltage was applied to the Pt wire to ingress the cytosol. Then, the capillary was withdrawn and re-positioned near the MS inlet for analysis. Typical spraying lasted for 2–4 s.

## Results and discussion

### Electrosyringe assisted sampling

To realize electrochemical ingress and a minimal salting effect on molecule ionization, a volatile electrolyte, NH<sub>4</sub>HCO<sub>3</sub> (100 mM, pH 7.8), was chosen as the extra and inner-capillary buffer. Since these two buffers were aqueous, no 2-phase system existed at the tip. As a result, the loading process could

not be monitored through the fluctuation of capillary resistance, which was well developed for a 2-phase system.<sup>40</sup> Therefore, a fluorescent probe, fluorescein ( $\lambda_{\text{ex/em}}$ : 494/521 nm), was added into the extra-capillary buffer as a label for the observation of the loading process. After applying a voltage of  $-3$  V at the metal wire for 60 s, the capillary was taken out of solution. The solution at the outer wall of the capillary dried in 5 min. However, due to the restricted evaporation of intra-capillary solution through the nano-orifice, no obvious decrease in buffer volume at the tip was observed under the microscope in 4 hours. Accordingly, the collection of bright-field and fluorescence images in 1–2 min was feasible, as shown in Fig. 2A and B. The contrast of the fluorescence image was adjusted to visualize the diffusion region of fluorescein inside the capillary. A fluorescence region  $\sim 13$   $\mu\text{m}$  in length was obtained, including a strong fluorescence spot (2  $\mu\text{m}$  in length) at the tip and a weak band ( $\sim 11$   $\mu\text{m}$  in length).

A control experiment was performed *via* the immersion of the nano-capillary in solution with fluorescein for 60 s without the application of voltage. No bright fluorescence spot was observed at the tip during ESI (Fig. S1†), supporting the electrochemical loading of aqueous solution into the capillary.

Upon the loading of fluorescein into the capillary, fluorescein moved up the capillary through free diffusion and electrochemical-migration in the presence of an electric field. The relatively high concentration of fluorescein at the front-end of the tip should be ascribed to equilibrium between loading and movement in the capillary. Meanwhile, the weak fluorescence band displays the diffusion of fluorescein along the capillary. This distribution of fluorescein in the capillary was validated *via* a simulation using Comsol software. The

boundary conditions and the simulated result are shown in the ESI (Fig. S2†). Similar to the experimental results, the concentration of species was high at the tip, and decreased gradually along the capillary. Based on the capillary dimensions (inner diameter: 130 nm; angle:  $4.2^\circ$ ) measured from scanning electron microscopy (SEM) images (Fig. 2C and D), the volume of the strong fluorescence spot (2  $\mu\text{m}$  in length) at the tip was calculated to be  $\sim 0.13$  fL. According to the concentration profile in Fig. S2B,† the amount of fluorescein in the diffusion band was calculated to be  $\sim 2.99$  fL. Eventually, a total of  $\sim 3.1$  fL of extra-capillary liquid was estimated to be loaded into the capillary, which was slightly less than the volume reported by Pourmand's group.<sup>42</sup> It was noted that this process might underestimate the real loading amount because some fluorescein that diffused further was not visualized and considered in the estimation. Despite this uncertainty regarding the loading amount, this electrosyringe should introduce the sample at the fL level into the nano-capillary.

### The electrospray mass spectrometric analysis of species in ammonium bicarbonate buffer

Five typical species, including tetraethylammonium hydrogen sulfate ( $\text{Et}_4\text{NHSO}_4$ ), hexamethylenetetramine ( $(\text{CH}_2)_6\text{N}_4$ ), glucose, sucrose and ascorbic acid, were dissolved in 100 mM  $\text{NH}_4\text{HCO}_3$  to examine electrospray mass spectrometric analysis. At this pH,  $\text{Et}_4\text{N}^+$  was positively charged, ascorbic acid losing a hydrogen ion was negatively charged, and  $(\text{CH}_2)_6\text{N}_4$ , glucose and sucrose remained neutral. Since the inner surface of the capillary was negatively charged, the negative voltage at the Pt wire should initiate EOF driving the positive ions, neutral molecules and negative ions in series into the nano-capillary. After the application of  $-3$  V for 60 s, mass spectra were recorded, as shown in Fig. 3A (positive mode) and B (negative mode). All the peaks in the spectra correspond to these five small molecules. This result confirmed the mass spectroscopic analysis of all these molecules with different charge states after electrochemical loading. Under these conditions, the detection limit was determined to be  $\sim 100$   $\mu\text{M}$  (over 0.05–0.1 fg) for these species, which was near to the mass limit of our instrument.

An increase in voltage or an extension to the time it is applied to the Pt wire during sampling should introduce more solution with the species into the nano-capillary. As expected, a higher integrated peak intensity is observed in the ESI (Fig. S3†). To exclude the possible contribution of molecular adsorption at the outer wall of the nano-capillary, the nano-capillary was positioned in the solution with these five species for 60 s without the application of voltage. No peaks associated with these molecules are seen in the ESI (Fig. S4†), supporting the reliability of electrosyringe-assisted electrospray mass spectrometric analysis.

To fully investigate the analytical ability of this mass spectrometric analysis, two representative proteins, met-enkephalin and angiotensin II, were analysed. As exhibited in the ESI (Fig. S5†), the peaks associated with these two proteins were observed in both of positive and negative modes. This result

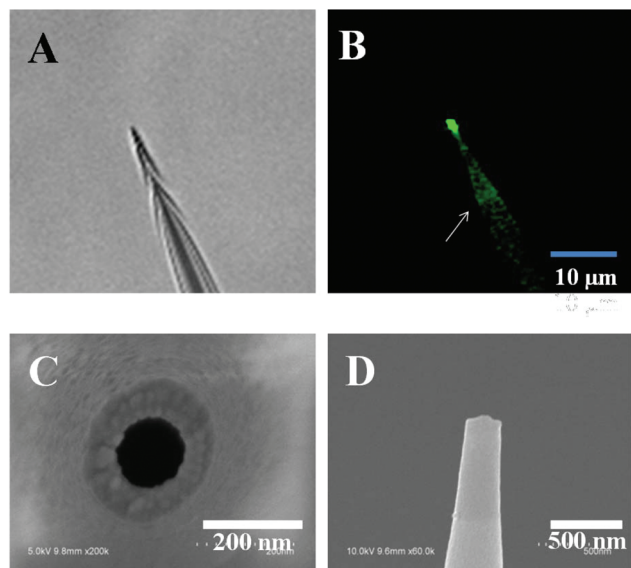


**Fig. 2** (A) Bright-field and (B) fluorescence images of the nano-capillary loaded with fluorescein after the application of  $-3$  V at the Pt wire for 60 s (the arrow labels the boundary of diffused fluorescein in the capillary); and (C, D) top and side views of the capillary tip using SEM.

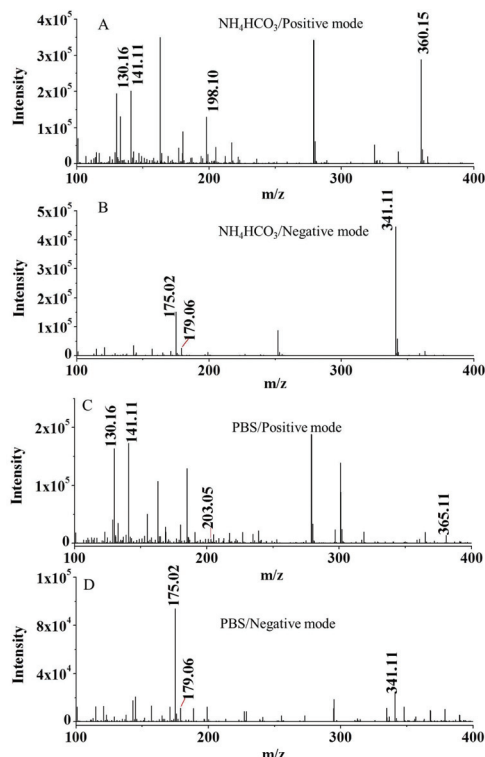


**Fig. 3** The mass spectra of samples in (A, B) 100 mM  $\text{NH}_4\text{HCO}_3$  and (C, D) PBS with 1 mM  $\text{Et}_4\text{NHSO}_4$ ,  $(\text{CH}_2)_6\text{N}_4$ , glucose, sucrose and ascorbic acid: (A, C) positive mode; (B, D) negative mode. The tentative substance assignments are shown in the ESI (Tables S1 and S2†).

reveals that this strategy could be applied for protein analysis, as well.

The ionization efficiency of molecules in electrosyringe assisted electrospray MS was evaluated. Glucose, a neutral molecule in our system, was chosen as the model. Different concentrations of glucose were manually filled and electrosprayed using nano-capillaries (orifice:  $\sim 130$  nm) and micro-capillaries (orifice:  $\sim 1$   $\mu\text{m}$ ). The peak intensities from the nano-capillaries and micro-capillaries are shown in the ESI (Fig. S6A†). At low concentrations of glucose, the peak intensity using the nano-capillary was less than that from the micro-capillary. However, the difference in the intensity became smaller with more glucose. With a concentration of 1 mM, the intensity using the nano-capillary was even slightly larger than that from the micro-capillary. Considering the smaller flow rate from the nano-capillary, the same order intensity from these two capillaries confirmed higher ionization efficiency from the nano-capillary. Based on a previous report, this enhancement should be attributed to the formation of smaller droplets with more charge from the smaller tip, which promotes ionization efficiency.<sup>31</sup>

Then, the intensity of 1 mM glucose though manual filling was compared with that from electrochemical loading, as shown in the ESI (Fig. S6B†). With a sampling time of over 120 s, the intensity collected from electrochemical loading reached 77% of the intensity from manual filling. The differ-

ence got smaller with more sample loaded into the nano-capillary, revealing the non-significant dilution of the sample during the whole analysis.

### The analysis of species in phosphate buffered saline

After the validation of electrosyringe assisted electrospray MS, a physiological buffer, 1 $\times$  PBS, with five species was used as a sample to mimic intracellular analysis. In this case, more salts will be loaded into the nano-capillary and the ionization will be depressed. Therefore, the analysis of species in this salted environment was critical for the achievement of subcellular mass spectrometric analysis. After the application of  $-3$  V to the metal wire for 60 s and electrospraying, the peaks associated with five species were observed in both positive and negative modes, as shown in Fig. 3C and D. Compared with the intensities when collected in  $\text{NH}_4\text{HCO}_3$ , except for sucrose, 43–85% intensity was maintained for the other four molecules suggesting the good tolerance of salts to the nano-capillary. Currently, several strategies have been developed for electrospray MS to minimize the salting effect on ionization, which could be adapted for our system to improve the detection sensitivity.<sup>46,47</sup> In the current work, the first realization of electrosyringe assisted electrospray mass spectrometric analysis in salted solution demonstrated the feasibility of nanometer scale cellular MS analysis.

### Single cell analysis

Single cell analysis was initiated *via* the insertion of the nano-capillary into single *Allium cepa* cells and HeLa cells. After the application of  $-3$  V to the Pt wire in the capillary for 60 s, the capillary was withdrawn from the *Allium cepa* cell and relocated near the inlet of the MS for electrospraying. The spectrum in Fig. 4A exhibits multiple peaks associated with the components of *Allium cepa* cells, including 5 fructans and 2 glucosides, which is consistent with previous results.<sup>22,48</sup> A detailed tentative assignment of the components in the cytosol

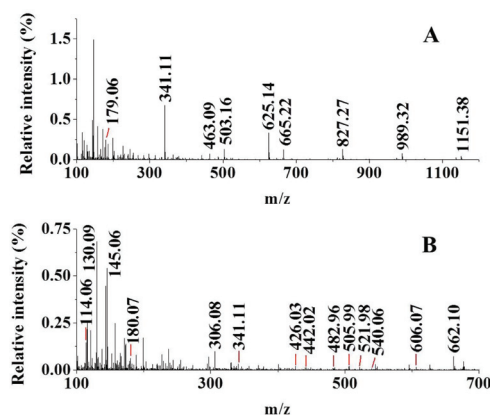


**Fig. 4** Negative-mode mass spectra of cytosol from (A) a single *Allium cepa* cell and (B) HeLa cell from using the electrosyringe. Tentative substance assignments for the cytosol are shown in the ESI (Tables S3 and 4†). The ion intensities were normalized using the total ion intensity.



is shown in the ESI (Table S3†). A control experiment without the application of a sampling voltage during capillary insertion into the cell did not exhibit any characteristic peaks associated with this type of cell, as shown in the ESI (Fig. S7†).

Similarly, the nano-capillary was inserted into one HeLa cell and analysis was performed. The spectrum and a detailed tentative assignment of the components are shown in Fig. 4B and the ESI (Table S4†). 19 components were profiled from one HeLa cell that had been observed from previous single cell MS analysis.<sup>22,48</sup> The successful collection of molecular information from single plant and mammalian cells supports the use of electrosyringe-assisted electrospray MS for nanometer scale cellular analysis.

### Analysis of single axons and dendrites

The molecular profiling of single axons, dendrites and bodies from living hippocampal neurons was performed using our electrosyringe-assisted electrospray MS. Typical images of the insertion of the nano-capillary into a single axon and dendrite are displayed in Fig. 5A and B. Following the same protocol, a voltage of  $-3$  V was applied for 60 s to sample the cytosol from one axon or dendrite. To ensure that there was minor interruption from insertion on cellular activity, the intracellular Ca concentration was monitored using a fluorescence probe, Fluo-3. No significant change in the fluorescence intensity before and after insertion confirmed the cellular activity. The spectra and detailed tentative assignments of the components from a single axon, dendrite and body are shown in Fig. 5C–E and the ESI (Table S5†). 14 components were profiled from the neuron body and most of these had been observed from neurons before.<sup>25,48,49</sup> Meanwhile, 11 and 12 out of 14 components were observed from the axon and dendrite, respectively, exhibiting the first molecular profiling of these two subtle cellular parts. The appearance of no peaks associated with CDP-ethanolamine, citicoline and cyclic ADP-ribose in the axon and CDP-ethanolamine and citicoline in the dendrite suggested lower concentrations of these species in the axon and dendrite.

A control experiment was performed by positioning the capillary tip outside the neuron for the sampling of extracellular liquid into the capillary. Similar to the spectrum collected from extracellular buffer outside HeLa cells, the spectrum shown in the ESI (Fig. S8†) did not display any characteristic peaks associated with the neuron. All these results support the accurate positioning of the capillary tip into the axon or dendrite for mass spectroscopic analysis. The relative standard deviations of the intensities of these species in these three cellular parts were calculated. Comparable deviation values as high as 59–99% were obtained for all these three parts. The observation of high heterogeneity of molecular content in axons and dendrites might offer information about different neuron behavior during information delivery.

Most importantly, higher levels of pyroglutamic acid and glutamic acid were revealed in the axon than in the body and dendrite, as shown in Fig. 5F. For the other species, no significant difference was observed between these three parts.

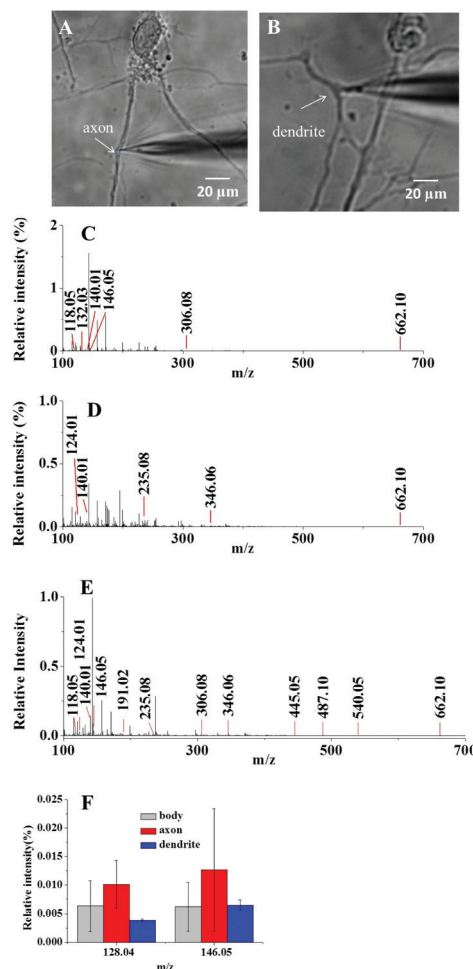


**Fig. 5** Images of the nanocapillary inserted into an axon (A) and a dendrite (B); the negative-mode mass spectra of femtolitre-scale cytosol from a single axon (C), dendrite (D) and body (E) – the ion intensities were normalized using the total ion intensities; and (F) the relative intensity of pyroglutamic acid ( $m/z$  128.04) and glutamic acid ( $m/z$  146.05) from an axon, a dendrite and a body from living neurons ( $n = 7$ ). The tentative substance assignments of aqueous species are shown in the ESI (Table S5†).

Classically, neuronal communication is fulfilled by neurotransmitters between synapses, which are created in the connection forms of axon–axon, dendrite–dendrite and axon–dendrite. All fast synaptic actions are mediated by the excitatory neurotransmitter glutamate and inhibitory neurotransmitters, such as gamma-aminobutyric acid (GABA) and glycine. Between axons and dendrites, axons are the major transmission elements of neurons, which extend distances from the cell body and carry signals to other neurons. Therefore, the observation of higher levels of glutamate and its precursor pyroglutamic acid in the axon than in the cell body and dendrite was expected. These results support our method as a special approach to elucidate the actual distribution of neurotransmitters and other components in neurons, which could reflect the actual physiological condition of neurons.

## Conclusions

Electrosyringe-assisted electrospray MS was established to achieve the first molecular profiling of single axons/dendrites/bodies in single living neurons. The successful analysis of multiple molecules in these cellular parts revealed different molecular distributions in neurons, which was ascribed to the different functions of axons and dendrites. Compared with current single cell ESI ionization methods using a micro-capillary, our approach couples a nano-capillary and electrosyringe to realize the sampling of subtle structures of cells, such as the axon and dendrite. The smaller sampling permits the gaining of subcellular information, which helps the understanding of cellular function. Further determination of the loading amount needs to be addressed for the quantification of species. Moreover, the continuous enhancement of ionization efficiency is urgently needed to unveil more species in axons and dendrites. Furthermore, some methods providing MS/MS fragments should be adapted with our system to offer more accurate molecular determination.

## Conflicts of interest

There are no conflicts to declare.

## Acknowledgements

This work was supported by the National Natural Science Foundation of China (no. 21327902, 21575060 and 81673720), and Major Programs of Natural Science Research in Universities of Jiangsu Province (15KJA360002).

## Notes and references

- 1 E. R. Kandel, *Principles of neural science*, Cambridge, McGrawHill, 4th edn, 2003.
- 2 D. Debanne, E. Campanac, A. Bialowas, E. Carlier and G. Alcaraz, *Physiol. Rev.*, 2011, **91**, 555–602.
- 3 S. S. Rubakhin, E. V. Romanova, P. Nemes and J. V. Sweedler, *Nat. Methods*, 2011, **8**, S20–S29.
- 4 W. Yang and R. Yuste, *Nat Methods*, 2017, **14**, 349–359.
- 5 B. Huang, M. Bates and X. W. Zhuang, *Annu. Rev. Biochem.*, 2009, **78**, 993–1016.
- 6 N. Ji, H. Shroff, H. Zhong and E. Betzig, *Curr. Opin. Neurobiol.*, 2008, **18**, 605–616.
- 7 P. Dedecker, C. Flors, J. I. Hotta, H. Uji-i and J. Hofkens, *Angew. Chem., Int. Ed.*, 2007, **46**, 8330–8332.
- 8 M. Maglione and S. J. Sigrist, *Nat. Neurosci.*, 2013, **16**, 790–797.
- 9 R. Y. Tsien, *Annu. Rev. Biochem.*, 1998, **67**, 509–544.
- 10 R. M. Hoffman, *Nat. Rev. Cancer*, 2005, **5**, 796–806.
- 11 R. Ferreira, A. K. Jarmusch, V. Pirro, C. M. Alfaro, A. F. González-Serrano, H. Niemann, M. B. Wheeler, R. A. Rabel, J. E. Hallett, R. Houser, A. Kaufman and R. G. Cooks, *Reprod., Fertil. Dev.*, 2015, **27**, 621–637.
- 12 R. Drissi, M. L. Dubois and F. M. Boisvert, *FEBS J.*, 2013, **280**, 5626–5634.
- 13 A. Oikawa and K. Saito, *Plant J.*, 2012, **70**, 30–38.
- 14 A. Amantonico, J. Y. Oh, J. Sobek, M. Heinemann and R. Zenobi, *Angew. Chem., Int. Ed.*, 2008, **47**, 5382–5385.
- 15 D. E. Warnock, E. Fahy and S. W. Taylor, *Mass Spectrom. Rev.*, 2004, **23**, 259–280.
- 16 L. Qiao, E. Tobolkina, A. Lesch, A. Bondarenko, X. Zhong, B. H. Liu, H. Pick, H. Vogel and H. H. Girault, *Anal. Chem.*, 2014, **86**, 2033–2041.
- 17 S. G. Boxer, M. L. Kraft and P. K. Weber, *Annu. Rev. Biophys.*, 2009, **38**, 53–74.
- 18 S. G. Ostrowski, C. T. Van Bell, N. Winograd and A. G. Ewing, *Science*, 2004, **305**, 71–73.
- 19 E. J. Lanni, S. S. Rubakhin and J. V. Sweedler, *J. Proteomics*, 2012, **75**, 5036–5051.
- 20 S. S. Rubakhin, W. T. Greenough and J. V. Sweedler, *Anal. Chem.*, 2003, **75**, 5374–5380.
- 21 S. Guenther, A. Römpf, W. Kummer and B. Spengler, *Int. J. Mass Spectrom.*, 2011, **305**, 228–237.
- 22 B. Shrestha and A. Vertes, *Anal. Chem.*, 2009, **81**, 8265–8271.
- 23 J. A. Stolee and A. Vertes, *Anal. Chem.*, 2013, **85**, 3592–3598.
- 24 J. A. Stolee, B. Shrestha, G. Mengistu and A. Vertes, *Angew. Chem., Int. Ed.*, 2012, **51**, 10386–10389.
- 25 X. Gong, Y. Zhao, S. Cai, S. Fu, C. Yang, S. C. Zhang and X. R. Zhang, *Anal. Chem.*, 2014, **86**, 3809–3816.
- 26 F. Chen, L. Lin, J. Zhang, Z. He, K. Uchiyama and J. M. Lin, *Anal. Chem.*, 2016, **88**, 4354–4360.
- 27 J. Deng, W. Li, Q. Yang, Y. Liu, F. Fang, Y. Guo, P. Guo, L. Lin, Y. Yang and T. Luan, *Anal. Chem.*, 2018, **90**, 6936–6944.
- 28 H. Mizuno, N. Tsuyama, T. Harada and T. Masujima, *J. Mass Spectrom.*, 2008, **43**, 1692–1700.
- 29 T. Fujii, S. Matsuda, M. L. Tejedor, T. Esaki, I. Sakane, H. Mizuno, N. Tsuyama and T. Masujima, *Nat. Protoc.*, 2015, **10**, 1445–1456.
- 30 K. Yamamoto, K. Takahashi, H. Mizuno, A. Negawa, K. Ishizaki, H. Fukaki, M. Ohnishi, M. Yamazaki, T. Masujima and T. Mimura, *Proc. Natl. Acad. Sci. U. S. A.*, 2016, **113**, 3891–3896.
- 31 J. T. Aerts, K. R. Louis, S. R. Crandall, G. Govindaiah, C. L. Cox and J. V. Sweedler, *Anal. Chem.*, 2014, **86**, 3203–3208.
- 32 R. M. Onjiko, S. A. Moody and P. Nemes, *Proc. Natl. Acad. Sci. U. S. A.*, 2015, **112**, 6545–6550.
- 33 C. Lombard-Banek, S. A. Moody and P. Nemes, *Angew. Chem., Int. Ed.*, 2016, **55**, 2454–2458.
- 34 R. M. Onjiko, E. P. Portero, S. A. Moody and P. Nemes, *Anal. Chem.*, 2017, **89**, 7069–7076.
- 35 H. Zhu, G. Zou, H. Wang, M. Zhuang, W. Xiong and G. M. Huang, *Proc. Natl. Acad. Sci. U. S. A.*, 2017, **114**, 2586–2591.

- 36 H. Zhu, N. Wang, L. Yao, Q. Chen, R. Zhang, J. Qian, Y. Hou, W. Guo, S. Fan, S. Liu, Q. Zhao, F. Du, X. Zuo, Y. Guo, Y. Xu, J. Li, T. Xue, K. Zhong, X. Song, G. M. Huang and W. Xiong, *Cell*, 2018, **173**, 1716–1727.
- 37 R. Zenobi and V. V. Deckert, *Angew. Chem., Int. Ed.*, 2000, **39**, 1746–1756.
- 38 O. S. Ovchinnikova, T. Tai, V. Bocharova, M. B. Okatan, A. Belianinov, V. Kertesz, S. Jesse and G. J. Van Berkell, *ACS Nano*, 2015, **9**, 4260–4269.
- 39 E. M. Yuill, N. Sa, S. J. Ray, G. M. Hieftje and L. A. Baker, *Anal. Chem.*, 2013, **85**, 8498–8502.
- 40 F. O. Laforge, J. Carpino, S. A. Rotenberg and M. V. Mirkin, *Proc. Natl. Acad. Sci. U. S. A.*, 2007, **104**, 11895–11900.
- 41 P. R. Pan, M. C. Xu, J. D. Burgess, D. C. Jiang and H. Y. Chen, *Proc. Natl. Acad. Sci. U. S. A.*, 2018, **115**, 4087–4092.
- 42 P. Actis, M. M. Maalouf, H. J. Kim, A. Lohith, B. Villozny, R. A. Seger and N. Pourmand, *ACS Nano*, 2014, **28**, 546–553.
- 43 E. N. Tóth, A. Lohith, M. Mondal, J. Guo, A. Fukamizu and N. Pourmand, *J. Biol. Chem.*, 2018, **293**, 4940–4951.
- 44 A. Chen, K. B. Lynch, J. Ren, Z. Jia, Y. Yang, J. J. Lu and S. Liu, *Anal. Chem.*, 2017, **89**, 10806–10812.
- 45 Y. Zhu, X. Duan, X. Cheng, X. Cheng, X. Li, L. Hang, P. Liu, S. Su, J. A. Duan, T. T. Dong, K. W. Tsim and F. Huang, *J. Ethnopharmacol.*, 2016, **193**, 423–432.
- 46 G. M. Huang, G. Li and R. G. Cooks, *Angew. Chem., Int. Ed.*, 2011, **50**, 9907–9910.
- 47 Z. Wei, S. Han, X. Gong, Y. Zhao, C. Yang, S. C. Zhang and X. R. Zhang, *Angew. Chem., Int. Ed.*, 2013, **52**, 11025–11028.
- 48 J. Hu, X. X. Jiang, J. Wang, Q. Y. Guan, P. K. Zhang, J. J. Xu and H. Y. Chen, *Anal. Chem.*, 2016, **88**, 7245–7251.
- 49 L. Zhang and A. Vertes, *Anal. Chem.*, 2015, **87**, 10397–10405.